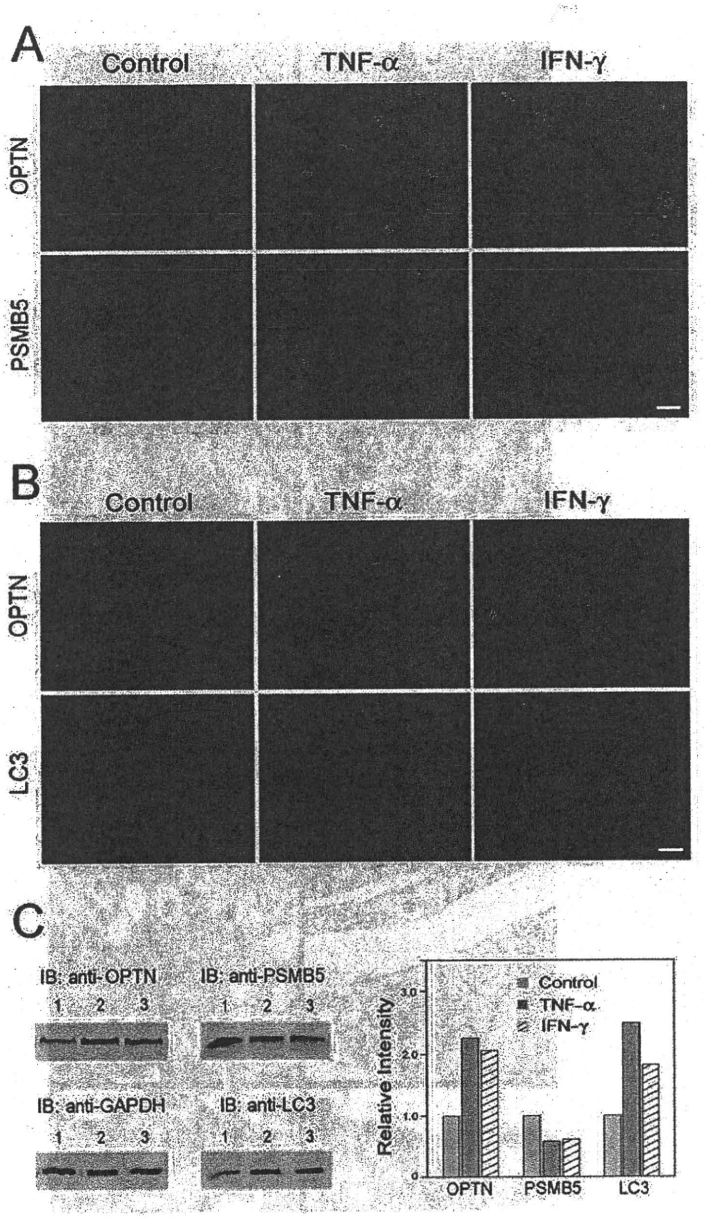

Figure 6

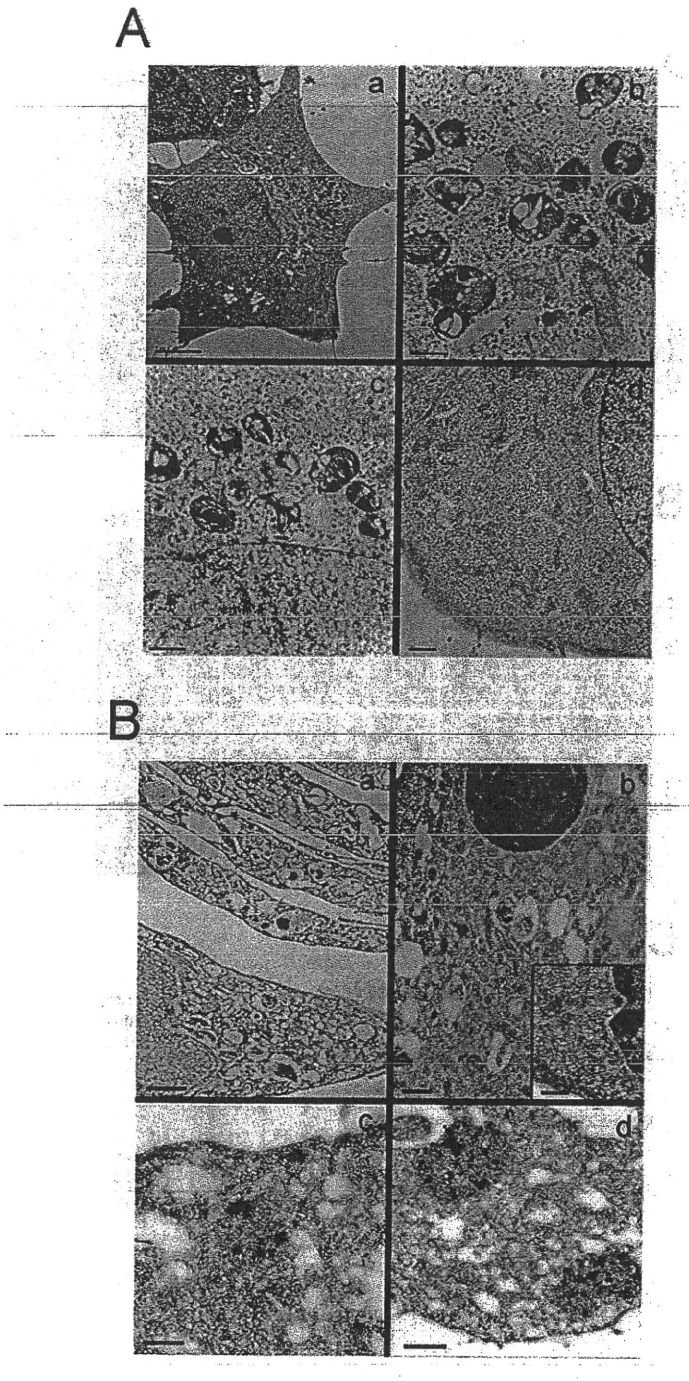

Figure 7

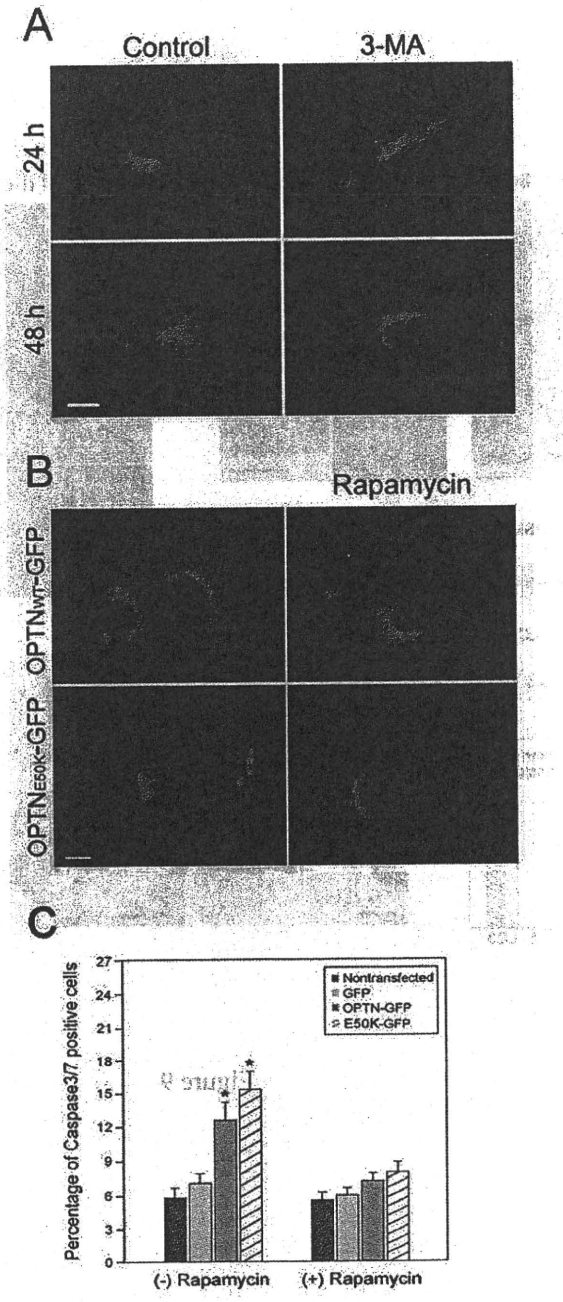

Figure 8

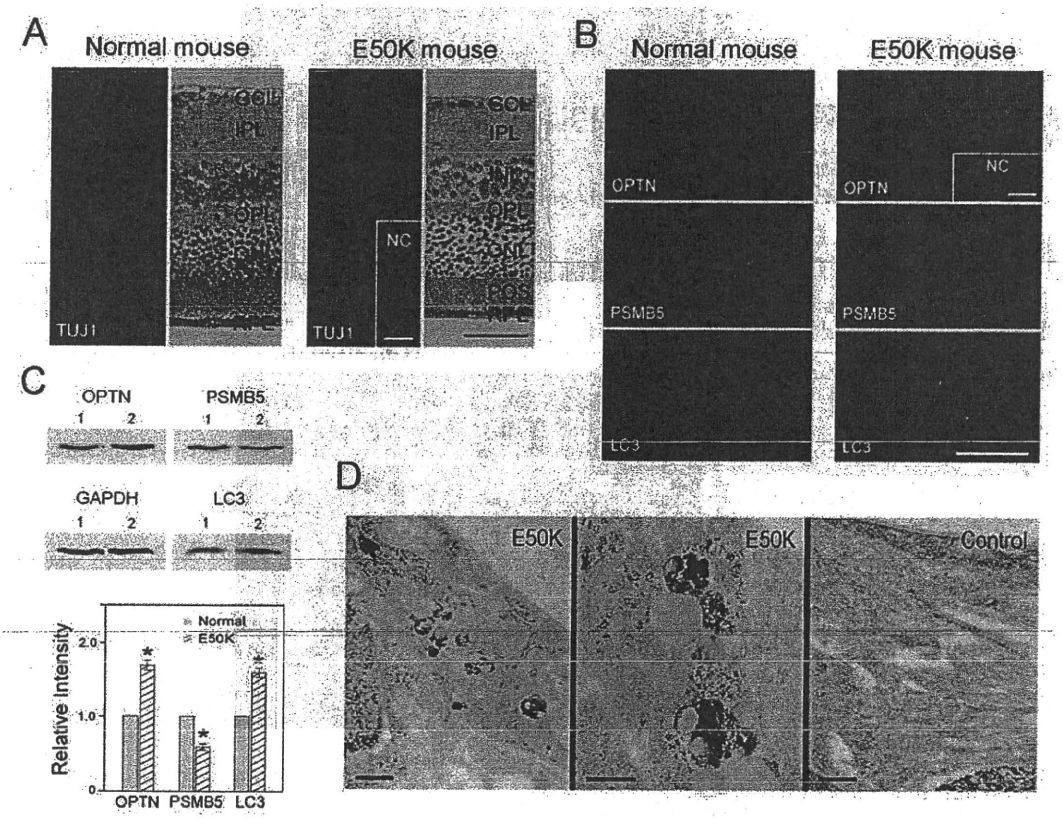

Figure 9

REPORT

Dominant Mutations in *RP1L1* Are Responsible for Occult Macular Dystrophy

Masakazu Akahori,[1] Kazushige Tsunoda,[1] Yozo Miyake,[1,2] Yoko Fukuda,[3] Hiroyuki Ishiura,[3] Shoji Tsuji,[3] Tomoaki Usui,[4] Tetsuhisa Hatase,[4] Makoto Nakamura,[5] Hisao Ohde,[6] Takeshi Itabashi,[1] Haru Okamoto,[1] Yuichiro Takada,[1] and Takeshi Iwata[1,*]

Occult macular dystrophy (OMD) is an inherited macular dystrophy characterized by progressive loss of macular function but normal ophthalmoscopic appearance. Typical OMD is characterized by a central cone dysfunction leading to a loss of vision despite normal ophthalmoscopic appearance, normal fluorescein angiography, and normal full-field electroretinogram (ERGs), but the amplitudes of the focal macular ERGs and multifocal ERGs are significantly reduced at the central retina. Linkage analysis of two OMD families was performed by the SNP High Throughput Linkage analysis system (SNP HiTLink), localizing the disease locus to chromosome 8p22-p23. Among the 128 genes in the linkage region, 22 genes were expressed in the retina, and four candidate genes were selected. No mutations were found in the first three candidate genes, methionine sulfoxide reductase A (*MSRA*), GATA binding 4 (*GATA4*), and pericentriolar material 1 (*PCM1*). However, amino acid substitution of p.Arg45Trp in retinitis pigmentosa 1-like 1 (*RP1L1*) was found in three OMD families and p.Trp960Arg in a remaining OMD family. These two mutations were detected in all affected individuals but in none of the 876 controls. Immunohistochemistry of RP1L1 in the retina section of cynomolgus monkey revealed expression in the rod and cone photoreceptor, supporting a role of RP1L1 in the photoreceptors that, when disrupted by mutation, leads to OMD. Identification of *RP1L1* mutations as causative for OMD has potentially broader implications for understanding the differential cone photoreceptor functions in the fovea and the peripheral retina.

Occult macular dystrophy (OMD) is an autosomal-dominant form of inherited macular dystrophy characterized by progressive decrease of visual acuity due to macular dysfunction, which was first reported by Y.M. et al. in 1989.[1–3] The disorder was called "occult" because of the fact that the macular dysfunction of this disease is hidden by a normal fundus appearance. Typical OMD, as described by Y.M. et al., is characterized by central cone dysfunction and in some cases rod dysfunction, leading to a loss of vision despite normal ophthalmoscopic appearance, normal fluorescein angiography, and normal full-field electroretinograms (ERGs). However, the amplitudes of the focal macular ERGs and multifocal ERGs are significantly reduced, indicating dysfunction of the central retina.[1,2,4] OMD is known for its broad range of age at disease onset, from 6 to 81 yrs. Brockhurst et al. have reported age at onset of four out of eight OMD patients at over 65 yrs[5] and similar findings have also been observed in earlier cases.[1,2] The patient III-3 in family 1 did not notice any visual disturbance in her right eye even at the age of 81 yrs.

The four families shown in Figure 1 demonstrate dominant inheritance of the OMD phenotype. None of the patients had ocular diseases other than OMD, except senile cataract or diabetic retinopathy. Control family members were confirmed to be normal via a complete ophthalmic examination including focal macular ERGs or multifocal ERGs. For this study, the ethics review committees of the National Hospital Organization Tokyo Medical Center, the Niigata University Graduate School of Medical and Dental Sciences, and the Nagoya University Medical School approved the study, and written informed consent was obtained from both affected and unaffected subjects.

Linkage analysis of OMD families 1 and 2 was performed. Eighteen individuals from family 1 and eleven individuals from family 2 were genotyped by Affymetrix's Genome-Wide Human SNP array 6.0 in accordance with the manufacturer's instructions (Affymetrix, Santa Clara, CA). DNA samples from family 2 were subjected to whole-genome amplification with the use of REPLI-g (QIAGEN, Tokyo, Japan) prior to SNP genotyping. With SNP HiTLink[6] used as a pipeline, SNPs with a Hardy-Weinberg p value > f 0.001, a call rate of 1, and a maximum confidence score > 0.02 were used for the analysis. SNPs with the minor allele frequency of 0 in controls were eliminated from the analysis. Parametric multipoint linkage analysis (autosomal-dominant model with a setting of liability classes; age-dependent penetrance of 0.19, 0.55, and 0.91 for 0–20, 21–40, and > 41 yrs old, respectively, and disease frequency of 0.000001) was performed with Allegro version 2,[7] intermarker distance from 80 kb to 120 kb with the use of SNP HiTLink. Because of the limitation of computational capacity, family 1 was divided into two branches (branch 1-1: descendants of II-1; branch

[1]National Institute of Sensory Organs, National Hospital Organization Tokyo Medical Center, 2-5-1 Higashigaoka, Meguro-ku, Tokyo 152-8902 Japan; [2]Aichi Medical University, 21 Yazakokarimata, Nagakute-cho, Aichi-gun, Aichi-ken, 489-1195 Japan; [3]Department of Neurology, Graduate School of Medicine, the University of Tokyo, 7-3-1, Hongo, Bunkyo-ku, Tokyo, 113-8655 Japan; [4]Division of Ophthalmology and Visual Science, Graduate School of Medical and Dental Sciences, Niigata University, Niigata, 757, Ichibancho, Asahimachidori, Niigata, 951-8510 Japan; [5]Nakamura Eye Clinic, 107-10, Kisei-cho, Nishi-ku, Nagoya, 452-0816 Japan; [6]Department of Ophthalmology, School of Medicine, Keio University, 35 Shinanomachi, Shinjuku-ku, Tokyo 160-8582, Japan
*Correspondence: iwatatakeshi@kankakuki.go.jp
DOI 10.1016/j.ajhg.2010.08.009.

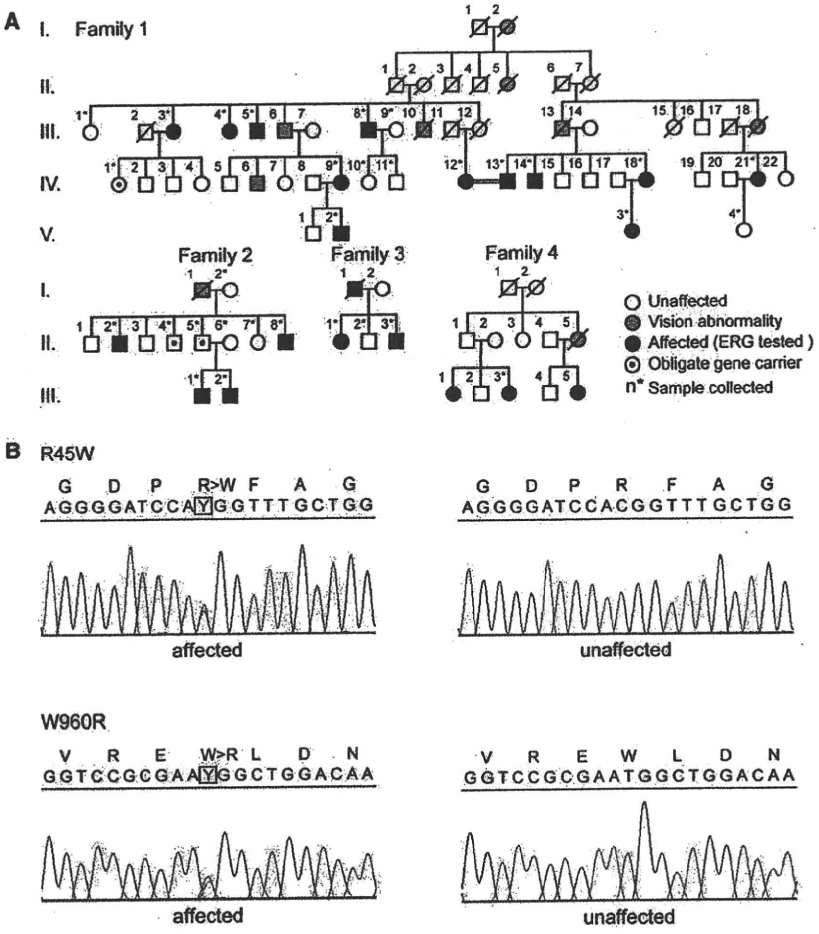

Figure 1. Autosomal OMD Families and DNA Sequencing of *RP1L1*

(A) The four families shown demonstrate dominant inheritance of the OMD phenotype. In all presented families, none of the patients had ocular diseases other than OMD, except senile cataract and diabetic retinopathy. Control family members were confirmed to be normal via a complete ophthalmic examination including focal macular ERGs or multifocal ERGs.

(B) DNA sequencing of both p.Arg45Trp and p.Trp960Arg mutations found in four independent families.

1-2: descendants of II-7) for multipoint linkage analysis. Haplotypes were reconstructed by Allegro.

The parametric linkage study of family 1 using SNP microarrays and SNP HiTLink mapped the disease locus to an approximately 10 Mb region of chromosome 8p22-p23 with a maximum LOD score of 3.77 (Figure 2). Parametric linkage analysis of affected individuals only produced similar results (Figure 3 and Figure S2 available online). A common haplotype between rs365309 and rs2632841 was shared by all of the affected individuals (Table 1). With the additional linkage study of family 2, the cumulative parametric multipoint LOD score rose to over 4 (Figure S1). A total of 128 known genes were found within the approximately 10 Mb linkage-associated region, containing 22 retina-expressed genes as candidates for mutational analyses. No mutations were found in the first three candidate genes, methionine sulfoxide reductase A (*MSRA*), GATA binding 4 (*GATA4*), and pericentriolar material 1 (*PCM1*). However, a c.362C>T (p.Arg45Trp) substitution in retinitis pigmentosa 1-like 1 (*RP1L1* [MIM 608581]) was found in all affected individuals in family 1. We further extended the mutational analysis of *RP1L1* to three other families with autosomal OMD, and we identified the p.Arg45Trp alteration in families 2 and 4 and a c.3107T>C (p.Trp960Arg) mutation in family 3 (Table 2). Additionally, known and unknown natural variants were found in *RP1L1*, as shown in Table S2. Unknown SNPs were submitted to the dbSNP database.

In these four families, all of the affected individuals carried one of the two mutations identified in this study, c.362C>T or c.3107T>C. We identified three apparently unaffected individuals carrying the p.Arg45Trp mutation, which suggest a reduced penetrance of the mutation or possibility a later onset of the disease for these individuals. Both mutations were absent in 1752 Japanese control chromosomes.

Immunohistochemistry of RP1L1 in the macula section of primate Cynomolgus monkeys (*Macaca fascicularis*) was performed. The eyes from a 6-yr-old normal male cynomolgus monkey were obtained from Tsukuba Primate Research Center, National Institute of Biomedical Innovation, Japan. All experimental procedures were approved by the Animal Welfare and Animal Care Committee of the National Institute of Biomedical Innovation, in compliance with guidelines of the Association for Research in Vision and Ophthalmology. Cynomolgus eyes were removed and immediately fixed overnight with 4% paraformaldehyde in 0.1 M phosphate buffer, pH 7.4. After washing in PBS, eyes were cryoprotected in the gradient sucrose dissolved in PBS and embedded into optimal cutting temperature (OCT) compound (Tissue Tek, Miles, IL, USA). Frozen retinal sections cut at 8 μm thickness with cryostat were incubated at 4°C with a 1:500 dilution of human RP1L1 polyclonal antibody raised against the N terminus of human RP1L1 (Santa Cruz Biotechnology, Santa Cruz, CA, USA). Immunofluorescence was visualized with Alexa 568 goat anti-rabbit IgG (Invitrogen, Carlsbad, CA, USA), Alexa 488 PNA (Invitrogen) for detection of cone photoreceptor, and DAPI (Invitrogen) for nuclear staining. Fluorescence images were analyzed with a confocal laser

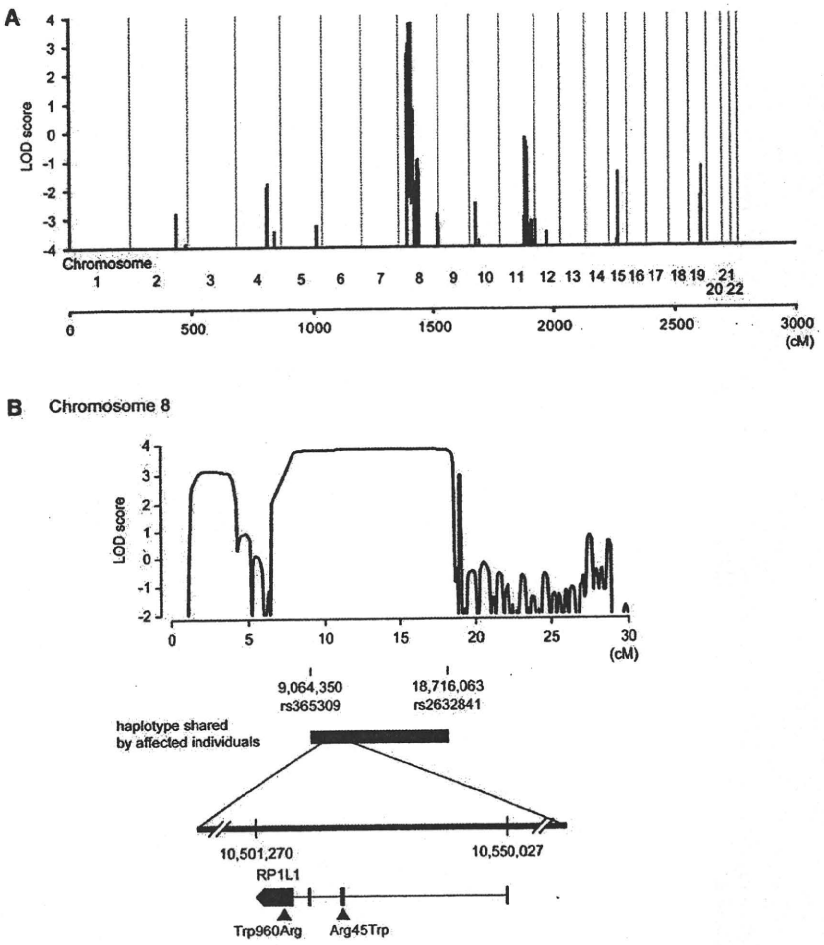

Figure 2. Linkage Analysis and Haplotype Analysis of Family 1

(A) Parametric multipoint linkage analysis of family 1. Horizontal axis indicates cumulative position (cM) from the short arm of chromosome 1. As a result of computational capacity, family 1 was divided into two branches for calculation of LOD scores. No other chromosomes except chromosome 8 yielded a positive LOD score.

(B) Parametric multipoint linkage analysis of family 1 and mutations in *RP1L1*. A maximum LOD score of 3.77 was obtained at 8p32.1-8p22. A haplotype bounded by rs365309 (physical position: 9,064,350 in the hg18 assembly of the UCSC Genome Browser) and rs2632841 (18,716,063) was shared by all affected individuals. Horizontal axis indicates the position (cM) on the short arm of chromosome 8. Vertical axis indicates the parametric multipoint LOD score. Mutations (p.Arg45Trp and p.Trp960Arg) are demonstrated.

microscope (Radiance 2000, Bio-Rad Laboratories, Hercules, CA, USA).

To our surprise, the immunohistochemistry of RP1L1 in the macula section of Cynomolgus monkeys revealed expression in retinal rod and cone photoreceptors by human RP1L1 antibody (Figure 3). This expression pattern is significantly different from the previous study of mouse RP1L1, in which RP1L1 was localized exclusively in axoneme of rods.[8] Furthermore, the human amino acid sequence is only 39% identical to that of the mouse, due to a lack of both polymorphic 16 amino acid repeats or a lack of the highly repetitive Glu-rich region, making mouse RP1L1 protein considerably shorter than the human protein, which may lead to different functional roles in the primate retina. Recent investigation of photoreceptor structure in OMD patients using advanced optical coherence tomography suggests that the predominant defect involves the cone photoreceptor.[9,10] Our optical coherence tomography observations also show loss of the cone outer segment tip and irregularity of the inner segment/outer segment junction in the center of the macula of all examined case individuals in family 1 (data not shown). Y.M. et al. have observed that not only cone but also rod sensitivity in the macula was abnormal in some of the older patients.[1,2] It is likely that the initial event may be macular cone specific but may later extend to rod abnormality. Further investigation of RP1L1 function is required in order to answer these clinical observations.

RP1L1 was originally cloned as a gene derived from common ancestor as retinitis pigmentosa 1 (*RP1* [MIM 180100]) on the same chromosome 8.[11,12] *RP1L1* shares 35% amino acid identity with *RP1*, a gene responsible for 5%–10% of autosomal-dominant retinitis pigmentosa (RP [MIM 268000]) worldwide.[13–15] When *RP1L1* was first identified, a number of attempts were made to identify mutations in *RP1L1* in various RP patients, with no success. The present study demonstrates that *RP1L1* mutation is responsible for OMD, but not for RP. Patients with RP carrying the most common RP1 alteration, p.Arg677X, exhibit night and peripheral vision disturbance beginning in the third decade of life. RP1 is found exclusively in the retina and is localized to both rods and cones. Rod-cone functional comparison in RP patients has indicated that rod sensitivity loss is at least 2 log units greater than cone sensitivity loss.[13] Thus phenotypic characteristics of RP caused by *RP1* mutations and those of OMD caused by *RP1L1* mutations perfectly agree with the different localizations of RP1 and RP1L1 in retina.

The outer segments of rod and cone photoreceptors are highly specialized cilia containing hundreds of disc membranes stacked in an orderly array along the photoreceptor axoneme. Previous studies have shown that RP1 is part of the axoneme and is required for this correct orientation and higher-order stacking of outer segment discs.[16] This is achieved by the interaction of RP1 with the

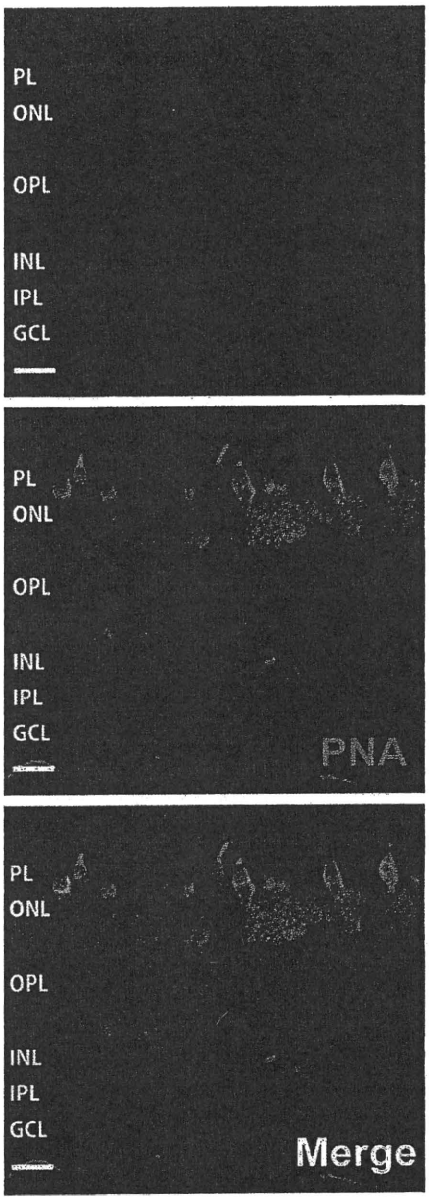

Figure 3. Immunohistochemistry of RP1L1 in the Cynomolgus Monkey Retina
Localization of RP1L1 in the rod and cone photoreceptors in the Cynomolgus monkey (*Macaca fascicularis*). Retina labeled with anti-human RP1L1 (red, top); same section labeled with retinal cone specific marker, peanut agglutinin lectin (PNA, green, middle); merged image (bottom). Yellow signal present in cone photoreceptor resulted from combination of the red signal of RP1L1 and the green signal of PNA. Cell nuclei were stained with DAPI (blue). PL, photoreceptor layer; ONL, outer nuclear layer; OPL, outer plexiform layer; INL, inner nuclear layer; IPL, inner plexiform layer; GCL, ganglion cell layer, Scale bars represent 20 μm.

microtubule in the connecting cilia.[17] RP1 contains microtubule-binding domains (amino acids 28–228) of neuronal microtubule-associated protein (MAP) doublecortin (DCX), which is required to maintain axoneme length and stability.[18] The RP1L1 p.Arg45Trp alteration resides in one of the two DCX domains (amino acids 33–113 and 147–228), which is required for interaction with RP1 to assemble and stabilize axonemal microtubules.[8] In primates, both RP1L1 and RP1 proteins may cooperatively function in the rod and cone photoreceptors to perform this task. The mutation in *RP1L1* is likely to dominantly affect the cooperative function with RP1 in rod and cone photoreceptors, given that in a previous publication, the *RP1L1* heterozygous knockout mice were reported to be normal whereas homozygous knockout mice were reported to develop subtle retinal degeneration. Our findings in OMD may shed light for further investigation of patients with cone dystrophy.

In conclusion, we identified *RP1L1* mutations that cause autosomal-dominant OMD, and furthermore, our findings revealed that *RP1L1* plays essential roles in the cone functions in human and that disruption of *RP1L1* function leads to OMD.

Supplemental Data

Supplemental Data include three figures and one table can be found with this article online at http://www.cell.com/AJHG/.

Acknowledgments

This research was supported in part by grants to Takeshi Iwata and Kazushige Tsunoda by the Ministry of Health, Labour, and Welfare of Japan. This work was also supported in part to Shoji Tsuji by KAKENHI (Grant-in-Aid for Scientific Research) on Priority Areas, Applied Genomics, the Global COE Program, and Scientific Research (A) from the Ministry of Education, Culture, Sports, Science and Technology of Japan.

Received: June 29, 2010
Revised: August 10, 2010
Accepted: August 12, 2010
Published online: September 9, 2010

Web Resources

The URLs for data presented herein are as follows:

dbSNP, www.ncbi.nlm.nih.gov/projects/SNP/
SNP HiTLink software, http://www.dynacom.co.jp/u-tokyo.ac.jp/snphitlink/

Accession Numbers

The dbSNP accession numbers for the SNPs reported in this paper are ss252841181 and ss252841182.

References

1. Miyake, Y., Ichikawa, K., Shiose, Y., and Kawase, Y. (1989). Hereditary macular dystrophy without visible fundus abnormality. Am. J. Ophthalmol. *108*, 292–299.

Table 1. Disease-Linked Haplotypes in Families 1 and 2

			Family 1					Family 2	
			Branch 1-1		Branch 1-2				
Probe Set ID	dbSNP rs ID	Position	III-8	IV-9	IV-13	IV-18	IV-21	II-2	III-2
SNP_A-8338925	rs365309	9,064,350	(A)	(A)	A	A	B	A	A
SNP_A-8281994	rs1530483	9,065,671	B	B	B	B	B	B	B
SNP_A-8360926	rs10086673	10,342,727	B	B	(B)	B	B	(A)	A
SNP_A-2082488	rs9329223	10,369,164	A	A	A	A	A	(B)	B
SNP_A-2013182	rs6601491	10,453,427	B	B	B	B	B	(A)	A
RP1L1 p.Arg45Trp	c.133C>T	10,517,989	T	T	T	T	T	T	T
SNP_A-8345504	rs10097570	10,586,268	A	A	A	A	(A)	(B)	B
SNP_A-1790165	rs10111051	10,590,882	A	A	A	A	(A)	(B)	B
SNP_A-8587750	rs2163379	10,769,460	A	A	A	(A)	A	(B)	B
SNP_A-8500791	rs7460507	11,006,485	B	B	B	B	B	A	A
SNP_A-8525908	rs9772321	12,536,010	A	A	A	A	A	A	A
SNP_A-8283296	rs1021087	13,500,502	A	(A)	(A)	A	A	B	B
SNP_A-8441723	rs6987209	14,501,302	B	B	B	B	B	B	B
SNP_A-2044287	rs7818067	15,580,087	A	A	A	A	A	A	A
SNP_A-4273924	rs6992112	16,689,526	A	A	A	A	A	A	(A)
SNP_A-8447659	rs471041	17,707,836	B	B	B	B	B	B	B
SNP_A-8399664	rs2638658	18,713,620	A	(A)	(A)	A	A	(B)	B
SNP_A-4233785	rs2632841	18,716,063	B	B	(B)	B	A	B	B

Disease-linked haplotypes of the two patients (IV-9 and III-8) who are descendants from II-1 (branch 1-1 of family 1), the three patients (IV-13, IV-18, and IV-21) who are descendants from II-7 (branch 1-2 of family 1), and the two patients (II-2 and III-2) from family 2 are shown. Haplotypes are unequivocally determined, except those with brackets that are inferred to minimize the number of recombination events. Disease-linked haplotypes of the two branches of family 1 are the same, confirming that all affected individuals in family 1 share the same haplotype. Recombination events in the family was observed at rs365309 (telomeric boundary) and at rs2632841 (centromereic boundary). When disease haplotypes are compared between families 1 and 2, who share the p.Arg45Trp mutation in *RP1L1* in common, disease-linked haplotypes flanking the *RP1L1* locus are different between these families, suggesting that the p.Arg45Trp mutation originated independently.

2. Miyake, Y., Horiguchi, M., Tomita, N., Kondo, M., Tanikawa, A., Takahashi, H., Suzuki, S., and Terasaki, H. (1996). Occult macular dystrophy. Am. J. Ophthalmol. *122*, 644–653.
3. Wildberger, H., Niemeyer, G., and Junghardt, A. (2003). Multifocal electroretinogram (mfERG) in a family with occult macular dystrophy (OMD). Klin. Monatsbl. Augenheilkd. *220*, 111–115.
4. Piao, C.H., Kondo, M., Tanikawa, A., Terasaki, H., and Miyake, Y. (2000). Multifocal electroretinogram in occult macular dystrophy. Invest. Ophthalmol. Vis. Sci. *41*, 513–517.
5. Brockhurst, R.J., and Sandberg, M.A. (2007). Optical coherence tomography findings in occult macular dystrophy. Am. J. Ophthalmol. *143*, 516–518.
6. Fukuda, Y., Nakahara, Y., Date, H., Takahashi, Y., Goto, J., Miyashita, A., Kuwano, R., Adachi, H., Nakamura, E., and Tsuji, S. (2009). SNP HiTLink: a high-throughput linkage analysis system employing dense SNP data. BMC Bioinfomatics *10*, 121.
7. Gudbjartsson, D.F., Thorvaldsson, T., Kong, A., Gunnarsson, G., and Ingolfsdottir, A. (2005). Allegro version 2. Nat. Genet. *37*, 1015–1016.
8. Yamashita, T., Liu, J., Gao, J., LeNoue, S., Wang, C., Kaminoh, J., Bowne, S.J., Sullivan, L.S., Daiger, S.P., Zhang, K., et al. (2009). Essential and synergistic roles of RP1 and RP1L1 in rod photoreceptor axoneme and retinitis pigmentosa. J. Neurosci. *29*, 9748–9760.
9. Park, S.J., Woo, S.J., Park, K.H., Hwang, J.M., and Chung, H. (2010). Morphologic photoreceptor abnormality in occult macular dystrophy on spectral-domain optical coherence tomography. Invest. Ophthalmol. Vis. Sci. *51*, 3673–3679.
10. Sisk, R.A., Berrocal, A.M., and Lam, B.L. (2010). Loss of foveal cone photoreceptor outer segments in occult macular dystrophy. Ophthalmic Surg Lasers Imaging *41*, 1–3.
11. Conte, I., Lestingi, M., den Hollander, A., Alfano, G., Ziviello, C., Pugliese, M., Circolo, D., Caccioppoli, C., Ciccodicola, A., and Banfi, S. (2003). Identification and characterization of the retinitis pigmentosa 1-like1 gene (RP1L1): a novel candidate for retinal degenerations. Eur. J. Hum. Genet. *11*, 155–162.
12. Bowne, S.J., Daiger, S.P., Malone, K.A., Heckenlively, J.R., Kennan, A., Humphries, P., Hughbanks-Wheaton, D., Birch, D.G., Liu, Q., Pierce, E.A., et al. (2003). Characterization of

Table 2. Summary of RP1L1 Mutations in Families with OMD

ID in Pedigree	Clinical Stage	Sex	Age at Diagnosis	Age at Onset in Estimation	Mutation	Best Corrected Visual Acuity (Right / Left)
1 III3	affected	F	81	50	c.362C>T	1.2 / 0.1
1 III4	affected	F	71	25	c.362C>T	0.4 / 0.5
1 III5	affected	M	74	30	c.362C>T	0.2 / 0.3
1 III8	affected	M	82	20	c.362C>T	0.2 / 0.2
1 IV1	unaffected	F	60	-	c.362C>T	1.2 / 1.2
1 IV9	affected	F	49	unknown	c.362C>T	1.2 / 1.2
1 IV12	affected	F	69	50	c.362C>T	0.1 / 0.07
1 IV13	affected	M	70	20	c.362C>T	0.1 / 0.1
1 IV14	affected	M	66	30	c.362C>T	0.2 / 0.3
1 IV18	affected	F	58	12	c.362C>T	0.1 / 0.1
1 IV21	affected	F	58	47	c.362C>T	0.1 / 0.4
1 V2	affected	M	20	13	c.362C>T	0.3 / 0.3
1 V3	affected	F	19	6	c.362C>T	0.2 / 0.15
2 II2	affected	M	69	unknown	c.362C>T	0.2 / 0.2
2 II4	unaffected	M	58	-	c.362C>T	1.0 / 1.0
2 II5	unaffected	M	55	-	c.362C>T	1.0 / 1.0
2 II8	affected	M	52	unknown	c.362C>T	0.2 / 0.3
2 III1	affected	M	23	23	c.362C>T	0.2 / 0.3
2 III2	affected	M	20	20	c.362C>T	0.3 /0.3
3 II1	affected	F	29	12	c.3107T>C	0.2 / 0.2
3 II3	affected	M	19	13	c.3107T>C	0.2 / 0.3
4 III3	affected	F	52	30	c.362C>T	0.15 / 0.15

Summary of individuals from autosomal OMD families 1–4, in whom p.Arg45Trp or p.Trp960Arg mutations of *RP1L1* were found. Three unaffected individuals at the age of 55–60 were found with the mutation. These individuals suggest a reduced penetrance of the mutation or a possible onset at a later age.

RP1L1, a highly polymorphic paralog of the retinitis pigmentosa 1 (RP1) gene, Mol. Vis. *9*, 129–137.

13. Pierce, E.A., Quinn, T., Meehan, T., McGee, T.L., Berson, E.L., and Dryja, T.P. (1999). Mutations in a gene encoding a new oxygen-regulated photoreceptor protein cause dominant retinitis pigmentosa. Nat. Genet. *22*, 248–254.
14. Sullivan, L.S., Heckenlively, J.R., Bowne, S.J., Zuo, J., Hide, W.A., Gal, A., Denton, M., Inglehearn, C.F., Blanton, S.H., and Daiger, S.P. (1999). Mutations in a novel retina-specific gene cause autosomal dominant retinitis pigmentosa. Nat. Genet. *22*, 255–259.
15. Jacobson, S.G., Cideciyan, A.V., Iannaccone, A., Weleber, R.G., Fishman, G.A., Maguire, A.M., Affatigato, L.M., Bennett, J., Pierce, E.A., Danciger, M., et al. (2000). Disease expression of RP1 mutations causing autosomal dominant retinitis pigmentosa. Invest. Ophthalmol. Vis. Sci. *41*, 1898–1908.
16. Liu, Q., Lyubarsky, A., Skalet, J.H., Pugh, E.N., Jr., and Pierce, E.A. (2003). RP1 is required for the correct stacking of outer segment discs. Invest. Ophthalmol. Vis. Sci. *44*, 4171–4183.
17. Liu, Q., Zuo, J., and Pierce, E.A. (2004). The retinitis pigmentosa 1 protein is a photoreceptor microtubule-associated protein. J. Neurosci. *24*, 6427–6436.
18. Gleeson, J.G., Allen, K.M., Fox, J.W., Lamperti, E.D., Berkovic, S., Scheffer, I., Cooper, E.C., Dobyns, W.B., Minnerath, S.R., Ross, M.E., and Walsh, C.A. (1998). Doublecortin, a brain-specific gene mutated in human X-linked lissencephaly and double cortex syndrome, encodes a putative signaling protein. Cell *92*, 63–72.

The American Journal of Human Genetics, Volume *87*

Supplemental Data

Dominant Mutations in *RP1L1* Are Responsible for Occult Macular Dystrophy

Masakazu Akahori, Kazushige Tsunoda, Yozo Miyake, Yoko Fukuda, Hiroyuki Ishiura, Shoji Tsuji, Tomoaki Usui, Tetsuhisa Hatase, Makoto Nakamura, Hisao Ohde, Takeshi Itabashi, Haru Okamoto, Yuichiro Takada, and Takeshi Iwata

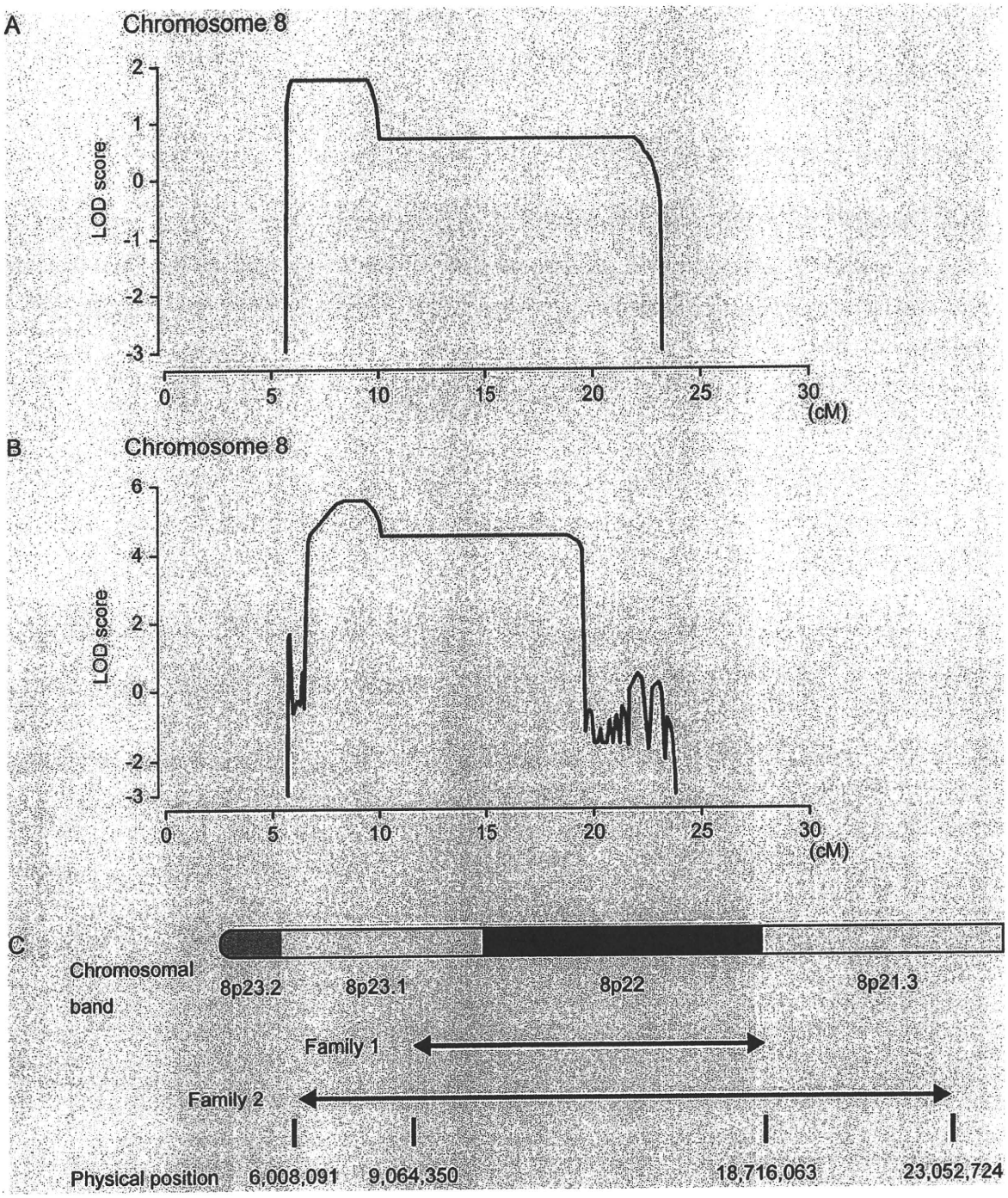

Figure S1. Linkage Analysis and Haplotype Analysis of Family 2

(A) Result of parametric multipoint analysis of Family 2. (B) Cumulative parametric multipoint LOD scores of Families 1 and 2. (C) Candidate regions based on the parametric analysis of Families 1 and 2.

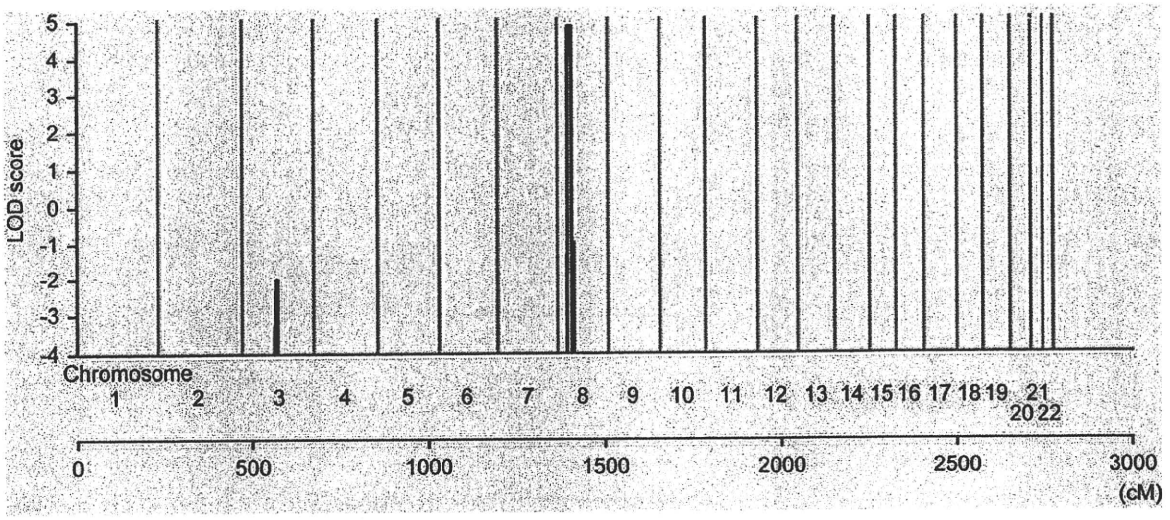

Figure S2. Parametric Linkage Analysis of Families 1 and 2 Using Affected Individuals Only

Cumulative maximum multipoint parametric lod score is shown. Horizontal axis represents the cumulative map position (cM) on the chromosomes 1-22. Family 1 was divided into 2 branches for calculation of LOD score as indicated.

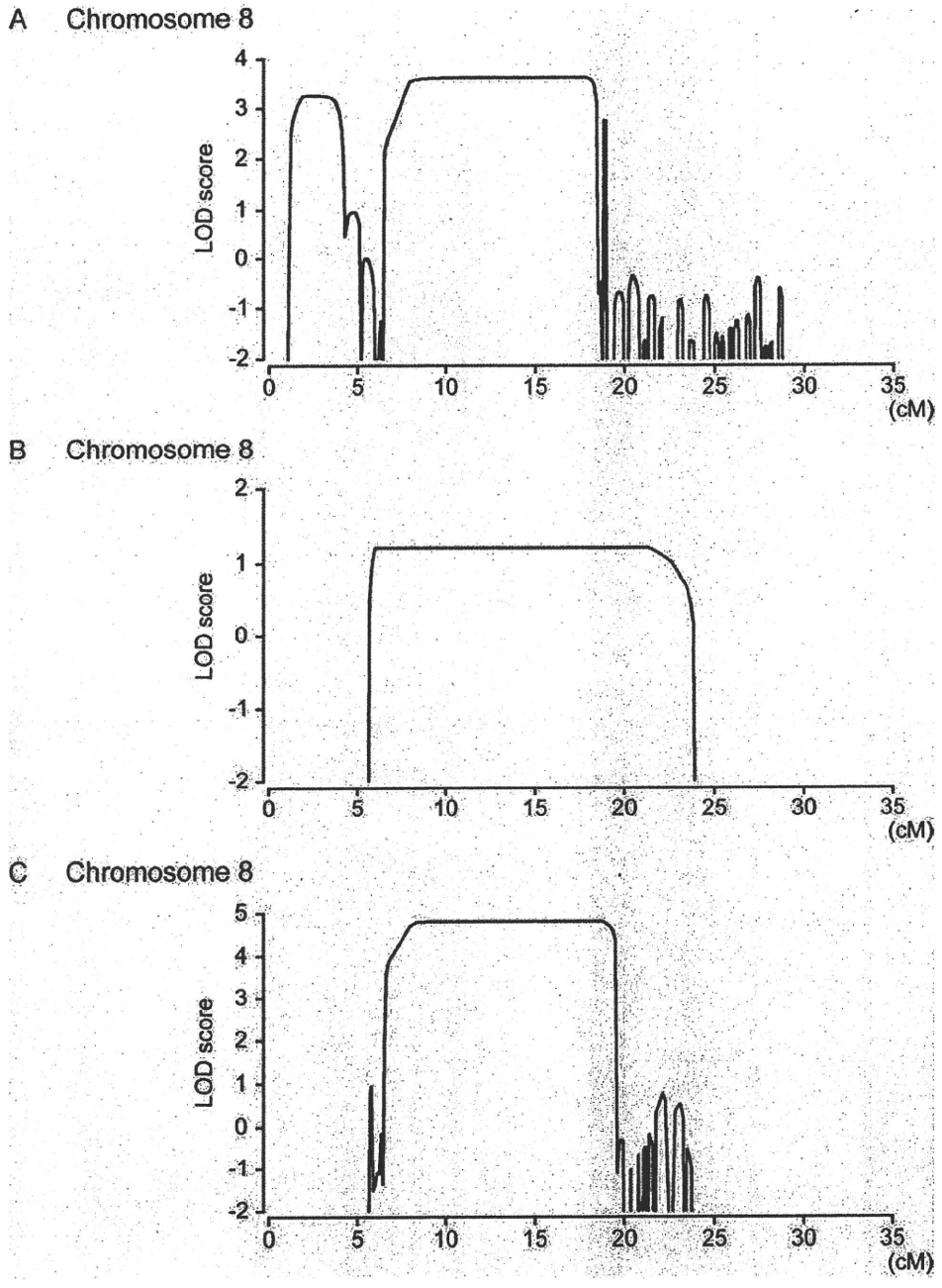

Figure S3. Parametric Linkage Analysis (Affected Individuals Only) at Loci on the Short Arm of Chromosome 8

Only the phenotypes of affected individuals are explicitly indicated in the analysis, while those of other individuals are indicated as "unknown". Maximum multipoint parametric lod scores for Families 1 (A) and 2 (B), and cumulative lod score for Families 1 and 2 (C) are shown. Since the family structure of Family 1 was too large for calculation, the family structure was divided into 2 branches for calculation of LOD score as indicated. Horizontal axis is the map position (cM) on the short arm of chromosome 8.

Table S1. Natural Variant in RP1L1 Sequence in OMD Families

cDNA change	Amino acid change	dbSNP.ID	Number of observed mutations/affected subjects (frequency)	Number of observed mutations/unaffected subjects (frequency)
c.518 G>C	E97Q	ss252841181	0/ 12 (0.00)	1/ 21 (0.05)
c.730 A>G	T167 synonymous	rs79329877	2/ 10 (0.20)	1/ 20 (0.05)
c.894 A>C	H222P	rs4388421	5/ 12 (0.42)	5/ 21 (0.24)
c.1769 G>A	G514S	rs74990397	3/ 12 (0.25)	3/ 21 (0.14)
c.2020 C>T	G597 synonymous	rs6996950	12/ 12 (1.00)	21/ 21 (1.00)
c.2497 C>T	N756 synonymous	rs57819090	4/ 12 (0.33)	3/ 21 (0.14)
c.2604 T>C	L792P	rs35602868	3/ 12 (0.25)	3/ 21 (0.14)
c.2807 C>T	R860W	rs62490856	3/ 12 (0.25)	2/ 21 (0.10)
c.3665 C>T	R1146W	rs4840502	12/ 12 (1.00)	21/ 21 (1.00)
c.4630 G>T	R1467S	rs4840498	12/ 12 (1.00)	21/ 21 (1.00)
c.4677 C>T	A1483V	rs62490855	1/ 12 (0.08)	0/ 21 (0.00)
c.4713 C>G	P1495R	rs4841399	10/ 12 (0.83)	21/ 21 (1.00)
c.5182 G>A	A1659 synonymous	ss252841182	1/ 12 (0.08)	3/ 21 (0.14)
c.5355 C>T	A1709V	rs13267180	3/ 12 (0.25)	3/ 21 (0.14)
c.5895 A>T	D1889V	rs28446662	9/ 12 (0.75)	18/ 19 (0.95)
c.6647 G>A	E2140K	rs72494282	5/ 12 (0.42)	5/ 21 (0.24)
c.6740 G>A	E2171K	rs4354268	2/ 12 (0.17)	1/ 21 (0.05)
c.6952 A>G	S2241 synonymous	rs56382513	11/ 12 (0.92)	20/ 21 (0.95)
c.7082 G>A	G2285R	rs55642448	11/ 12 (0.92)	21/ 21 (1.00)

Nucleotides and amino acid are numbered as in GenBank accesssion number NM_178857 and NP_849188.4, respectively. Sequencing of the CDS excluding repeat site (approximately 3960 to 4320 and 5980 to 6480; NM_178857) of RP1L1 in OMD family members.

OPEN ACCESS Freely available online

PLoS one

Modeling Retinal Degeneration Using Patient-Specific Induced Pluripotent Stem Cells

Zi-Bing Jin[1,2☯], Satoshi Okamoto[1☯], Fumitaka Osakada[3], Kohei Homma[1], Juthaporn Assawachananont[1], Yasuhiko Hirami[1], Takeshi Iwata[4], Masayo Takahashi[1,5*]

1 Laboratory for Retinal Regeneration, RIKEN Center for Developmental Biology, Kobe, Japan, 2 School of Optometry and Ophthalmology, Eye Hospital, Wenzhou Medical College, Wenzhou, China, 3 Systems Neurobiology Laboratory, The Salk Institute for Biological Studies, La Jolla, California, United States of America, 4 National Institute of Sensory Organs, National Hospital Organization Tokyo Medical Center, Tokyo, Japan, 5 Center for iPS Research and Application, Kyoto University, Kyoto, Japan

Abstract

Retinitis pigmentosa (RP) is the most common inherited human eye disease resulting in night blindness and visual defects. It is well known that the disease is caused by rod photoreceptor degeneration; however, it remains incurable, due to the unavailability of disease-specific human photoreceptor cells for use in mechanistic studies and drug screening. We obtained fibroblast cells from five RP patients with distinct mutations in the *RP1*, *RP9*, *PRPH2* or *RHO* gene, and generated patient-specific induced pluripotent stem (iPS) cells by ectopic expression of four key reprogramming factors. We differentiated the iPS cells into rod photoreceptor cells, which had been lost in the patients, and found that they exhibited suitable immunocytochemical features and electrophysiological properties. Interestingly, the number of the patient-derived rod cells with distinct mutations decreased *in vitro*; cells derived from patients with a specific mutation expressed markers for oxidation or endoplasmic reticulum stress, and exhibited different responses to vitamin E than had been observed in clinical trials. Overall, patient-derived rod cells recapitulated the disease phenotype and expressed markers of cellular stresses. Our results demonstrate that the use of patient-derived iPS cells will help to elucidate the pathogenic mechanisms caused by genetic mutations in RP.

Citation: Jin Z-B, Okamoto S, Osakada F, Homma K, Assawachananont J, et al. (2011) Modeling Retinal Degeneration Using Patient-Specific Induced Pluripotent Stem Cells. PLoS ONE 6(2): e17084. doi:10.1371/journal.pone.0017084

Editor: Mark Mattson, National Institute on Aging Intramural Research Program, United States of America

Received October 28, 2010; **Accepted** January 15, 2011; **Published** February 10, 2011

Funding: This study was supported by the grant from the Ministry of Health, Labour and Welfare, Japan (#H21-Nanchi-Ippan-216). The funders had no role in study design, data collection and analysis, decision to publish, or preparation of the manuscript.

Competing Interests: The authors have declared that no competing interests exist.

* E-mail: mretina@cdb.riken.jp

☯ These authors contributed equally to this work.

Introduction

Retinitis pigmentosa (RP) leads inevitably to visual impairment due to irreversible retinal degeneration, specifically of primary rod photoreceptors. The condition causes night blindness and visual field defects. The disease onset spans a wide range of ages, but RP most often occurs in late life. There is no treatment that allows patients to avoid deterioration of visual function. RP encompasses a number of genetic subtypes, with more than 45 causative genes and a large number of mutations identified thus far. The genetic heterogeneity of RP suggests a diversity of disease mechanisms, which remain largely unclear. Furthermore, for many of the RP subtypes, no appropriate animal models are available. Although large clinical trials have been conducted with α-tocopherol and β-carotene, these studies found no statistically significant change of visual function in RP patients [1,2]. The underlying mutations causing disease in the patients tested in the clinical trials were not revealed, and the variability of individual responses to these drugs is unknown. One of the reasons why these clinical trials failed to examine the effectiveness of drugs is that the effect of a drug may be different between patients with different underlying mutations.

Induced pluripotent stem (iPS) cells reprogrammed from somatic cells [3,4] have enabled us to easily generate patient-derived terminally differentiated cells *in vitro* [5–7]. We have successfully induced differentiation of photoreceptor cells from both human embryonic stem (ES) cells [8] and iPS cells [9,10]. Modeling pathogenesis and treatment *in vitro* using patient iPS cell-derived photoreceptors will elucidate disease mechanisms; circumvent problems related to differences among species that arise when using animal models; decrease patient risk; and reduce the cost of early-stage clinical trials. Here, we generated iPS cells from RP patients with different mutations and demonstrated the potential of patient-derived photoreceptors for disease modeling.

Materials and Methods

RP patients and genetic mutations

The protocol of this study adhered to the tenets of the Declaration of Helsinki. The study was approved by the ethical committees of the Institute of Biomedical Research and Innovation Hospital and the RIKEN Center for Developmental Biology, Japan. Written informed consent from all patients was obtained. We selected five RP patients from four families whose disease-causing mutations have been identified (**Fig. 1A–D and Fig. S1**). Of the five RP patients in this study, three late-onset patients carried the following mutations: 721Lfs722X in *RP1*, W316G in *PRPH2*, and G188R in *RHO*. Two relatively early-onset patients from the same family carried a H137L mutation in *RP9*, which we

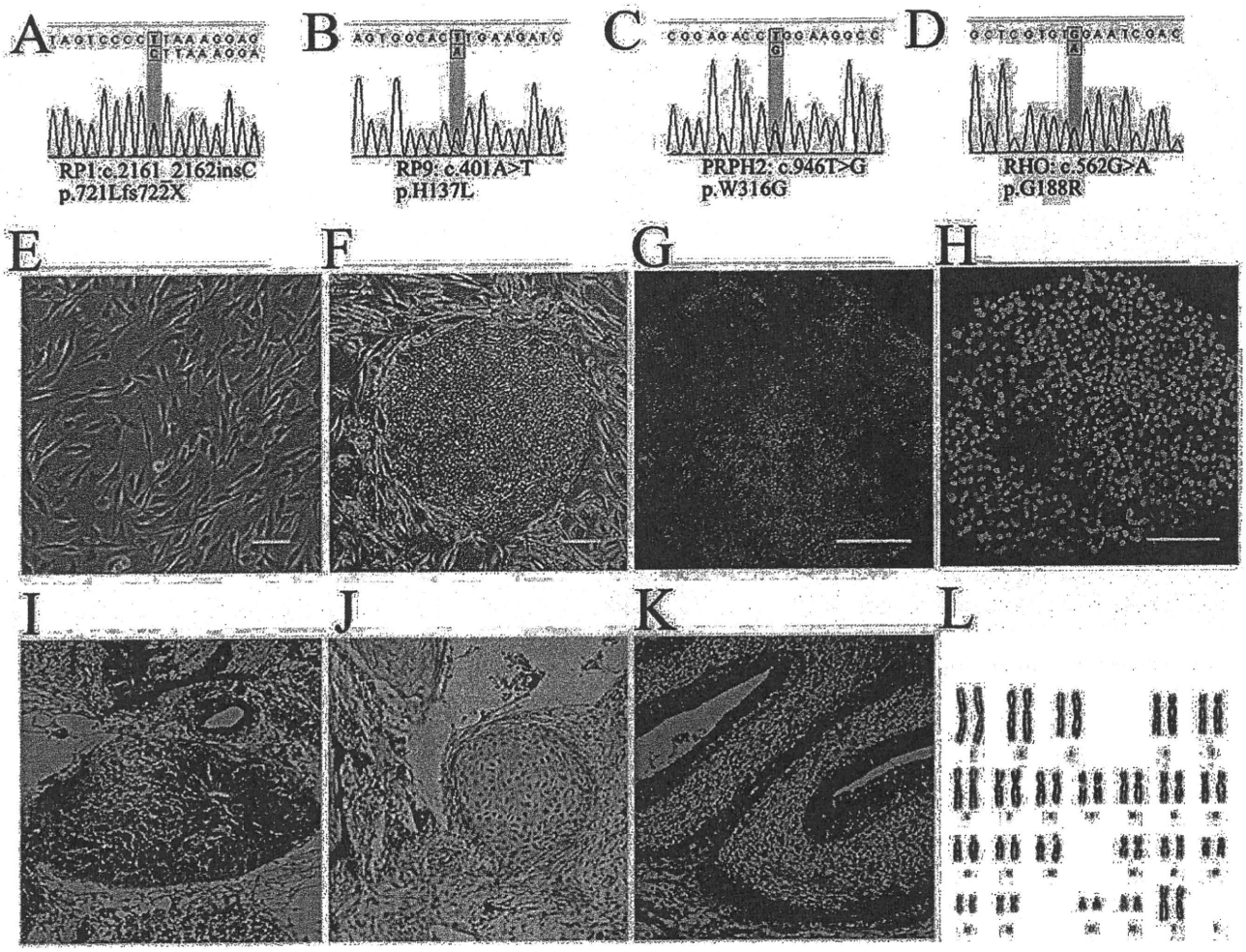

Figure 1. iPS cells derived from RP patients. Mutations identified in patients K21 (RP1) (**A**), K11 and K10 (RP9) (**B**), P101 (PRPH2) (**C**), and P59 (RHO) (**D**). Patient-derived fibroblast cells (**E**) were reprogrammed into iPS cells (**F**). The iPS cells expressed SSEA-4 (**G**) and Nanog (**H**). A teratoma formation test confirmed iPS cells' ability to generate all three germ layers: endoderm (**I**), mesoderm (**J**) and ectoderm (**K**). Karyotype analysis (**I**). Scale bars, 50 μm.
doi:10.1371/journal.pone.0017084.g001

confirmed by both genomic and cDNA sequencing (**Fig. S2**). All patients showed typical manifestations of RP (**Tab. S1**). Peripheral blood obtained from patients was used for DNA isolation. A comprehensive screening of disease-causing genes was carried out as described previously [11]. For the RP9 mutation, total RNA was isolated from fresh blood samples and iPS cells, and synthesized cDNA was subjected to PCR and direct sequencing to confirm whether the mutation was located in the *RP9* gene or the pseudo-RP9 gene (paralogous variant). Both fibroblast and iPS cells were analyzed to re-confirm the identified mutation.

iPS cells generation

To generate iPS cells, retroviral transduction of Oct3/4, Sox2, Klf4, and c-Myc into patient-derived fibroblast cells was carried out as described previously [3]. Established iPS cell lines were maintained on a feeder layer of mitomycin C-treated SNL cells (a murine-derived fibroblast STO cell line expressing the neomycin-resistance gene cassette and LIF) in a humidified atmosphere of 5% CO_2 and 95% air at 37°C. Cells were maintained in DMEM-F12 supplemented with 0.1 mM non-essential amino acids, 0.1 mM 2-mercaptoethanol, 2 mM L-glutamine, 20% KnockOut Serum Replacement (KSR), and 4 ng/ml basic fibroblast growth factor (Upstate Biotechnology).

Transgene quantification

To examine the copy number of transgenes integrated into the host genome, DNA was isolated and quantitative detection of viral transgenes was performed using real-time PCR. The endogenous gene was used as a control. Before quantitative PCR, a standard curve for each primer and/or probe set was determined using a set of plasmid DNA dilutions. Taqman qPCR to detect integrated OCT3/4, KLF4, and MYC was performed using 20 μl reactions consisting of 10 μl TaqMan Master Mix with uracil N-glycosylase, 4.9 μM primers, 250 nM probe, and 1 μl of the DNA sample. Quantification of viral SOX2 was assayed using SYBR Green.

Teratoma formation

Animal protocols were approved by the RIKEN Center for Developmental Biology ethical committee (No. AH18-05). A total of 10^7 trypsinized iPS cells were injected subcapsularly into the testis of SCID mice (two mice per iPS cell line). Four weeks later, the testis was fixed and sectioned for H&E staining.

Immunocytochemistry

Cells were fixed with 4% paraformaldehyde for 15 min at 4°C and then permeabilized with 0.3% Triton X-100 for 45 min. After 1 h blocking with 5% goat serum, cells were incubated with primary antibodies overnight at 4°C and subsequently with secondary antibodies for 1 h at room temperature. The primary and second antibodies used are listed in **Tab. S2**.

Karyotype analysis

Karyotype analysis of the iPS cell chromosomes was carried out using a standard G-band technique (300–400 band level).

Photoreceptor differentiation and drug testing

In vitro differentiation of rod photoreceptor cells was performed as previously reported [8], but with a minor modification. To find a KSR optimal for retinal differentiation, lot testing was conducted before differentiation. iPS colonies were dissociated into clumps with 0.25% trypsin and 0.1 mg/ml collagenase IV in PBS containing 1 mM $CaCl_2$ and 20% KSR. Feeder cells were removed by incubation of the iPS cell suspension on a gelatin-coated dish for 1 h. iPS clumps were moved to a non-adhesive MPC-treated dish (NUNC) in maintenance medium for 3 days, in 20% KSR-containing differentiation medium (DMEM-12 supplemented with 0.1 mM non-essential amino acids, 0.1 mM 2-mercaptoethanol, 2 mM L-glutamine) for 3 days, then in 15% KSR-containing differentiation medium for 9 days, and finally in 10% KSR-containing medium for 6 days. Cells were treated with Lefty-A and Dkk-1 during floating culture. At day 21, the cells were plated en bloc on poly-D-lysine/laminin/fibronectin−coated 8-well culture slides (BD Biocoat) at a density of 15–20 aggregates/cm^2. The cells were cultured in 10% KSR-containing differentiation medium until day 60. Cells were further treated with 100 nM retinoic acid (Sigma) and 100 μM taurine (Sigma) in photoreceptor differentiation medium (GMEM, 5% KSR, 0.1 mM non-essential amino acids, 0.1 mM 2-mercaptoethanol, 1 mM pyruvate, N2 supplement, and 50 units/ml penicillin, 20 μg/ml streptomycin). Differentiated cells from both normal and patient iPS cells were treated with 100 μM α-tocopherol, 200 μM ascorbic acid and 1.6 μM β-carotene starting at differentiation day 120. One week later, cells were fixed for immunostaining.

Electrophysiological recording

Recombinant lentiviral vectors expressing GFP under the control of the Nrl or RHO promoters were generated in HEK293t cells (RIKEN Cell Bank), and differentiated cells were infected with virus on day 90. Cells expressing GFP were targeted for patch clamp recordings. Voltage-clamp recordings were performed with 12–15 MΩ glass electrodes. Signals were amplified using Multiclamp 700B amplifiers (Molecular Devices). The internal solution was 135 mM K-gluconate, 10 mM HEPES, 3 mM KCl, 0.2 mM EGTA, 2.5 mM $MgCl_2$, 5 mM adenosine 5′-triphosphate, 0.3 mM guanosine-5′-triphosphate, 0.06 mM Alexa Fluor 594 (Molecular probes), adjusted to pH 7.6 with KOH. The retinal cells were perfused with oxygen-bubbled external medium: 23 mM $NaHCO_3$, 0.5 mM KH_2PO_4, 120 mM NaCl, 3.1 mM KCl, 6 mM Glucose, 1 mM $MgSO_4$, 2 mM $CaCl_2$, and 0.004% Phenol red. The medium was heated to 37°C with a temperature controller (Warner Instruments).

Cell count and statistical analysis

Differentiated cells visualized with specific antibodies were counted blindly by an independent observer. Data are expressed as means ± s.e.m. The statistical significance of differences was determined by one-way ANOVA followed by Tukey's test or Dunnett's test, or by two-way ANOVA followed by Bonferroni test using the GraphPad Prizm software. Probability values less than 0.05 were considered significant.

Results

Generation of iPS cell lines from patients with RP

Mutations identified in the five patients were confirmed by bi-directional sequencing (**Fig. S1**). Through genotyping of four patients and two normal relatives in the RP9 family, we found the H137L mutation in the *RP9* gene co-segregated with the disease, strongly indicating that the mutation is indeed the genetic cause of the disease. We cultured fibroblasts from skin samples of these patients on gelatin-coated dishes (**Fig. 1E**) and infected them with retroviral vectors encoding *OCT3/4* (also known as *POU5F1*), *SOX2*, *KLF4*, and *c-MYC*, using a previously established method [3]. Each mutation was re-confirmed in both fibroblasts and iPS cells. Established iPS colonies showed human embryonic stem cell-like morphology (**Fig. 1F and Fig. S3A**) and expressed pluripotency markers (**Fig. 1C–D**). We selected iPS cell lines for each patient using multiple criteria. First, we excluded iPS cell lines in which spontaneous differentiation occurred repeatedly during maintenance (**Fig. S3B**). We chose iPS colonies that maintained morphologies similar to those of human ES cells through more than 10 passages. Second, we quantified the transgene copy number and selected iPS cell lines with the fewest integrations, as the risk of gene disruption through random insertion increases with the number of transgenes (**Fig. S4A–E**). Third, in order to select iPS cell lines with full pluripotency, we verified the ability to form teratomas. Teratomas formed by injecting iPS colonies into the testis *in vivo* showed contributions to all three embryonic germ layers: ectoderm, mesoderm, and endoderm (**Fig. 1E–G**). Finally, karyotype analysis was carried out to examine the chromosome integrity. The patient-iPS cells showed normal karyotypes after extended passage, indicating chromosomal stability (**Fig. 1H**). These results provide *in vitro* and *in vivo* functional proof of pluripotency for RP patient-derived iPS cells.

Generation of patient-specific retinal photoreceptor

We previously demonstrated *in vitro* differentiation of retinal photoreceptor cells from wild-type human ES [8] and iPS cells [9,10] using a stepwise differentiation method known as serum-free culture of embryoid body-like aggregates [12]. We first evaluated the differentiation efficiency of three selected iPS cell lines of the five patients (**Fig. 2A**). Retinal progenitor, photoreceptor precursor, retinal pigment epithelium (RPE) and rod photoreceptor cells were sequentially induced (**Fig. 2B–K**), consistent with our previous studies [8–10,12]. All patient-derived iPS cell lines differentiated into RPE cells that form ZO-1+ tight junctions on differentiation day 60, with timing, morphology, and efficiency similar to that of wild-type iPS cells (**Fig. 2D–E; Fig. S5**). Immature photoreceptors expressing Crx and Recoverin (day ~60) were observed as clusters in the colonies (**Fig. S6A–B**). The patient-iPS cells also differentiated into blue Opsin+ or red/green Opsin+ cone photoreceptor cells (**Fig. 2H** and data not shown). Immunostaining of Rhodopsin (a marker of mature rod photoreceptors) revealed no Rhodopsin+ cells at differentiation day 100 (data not shown). Rhodopsin+ cells appeared at differentiation day 120 with a stable efficiency of the three independent iPS cell lines from each patient (**Fig. 2K,N and Fig. S6C**). Additionally, 15.1±0.60% and 13.3±1.65% cells were positive for Recoverin (a conventional marker for both rod, cone photoreceptors and cone bipolar cells) in K21- and K11-iPS cells, respectively

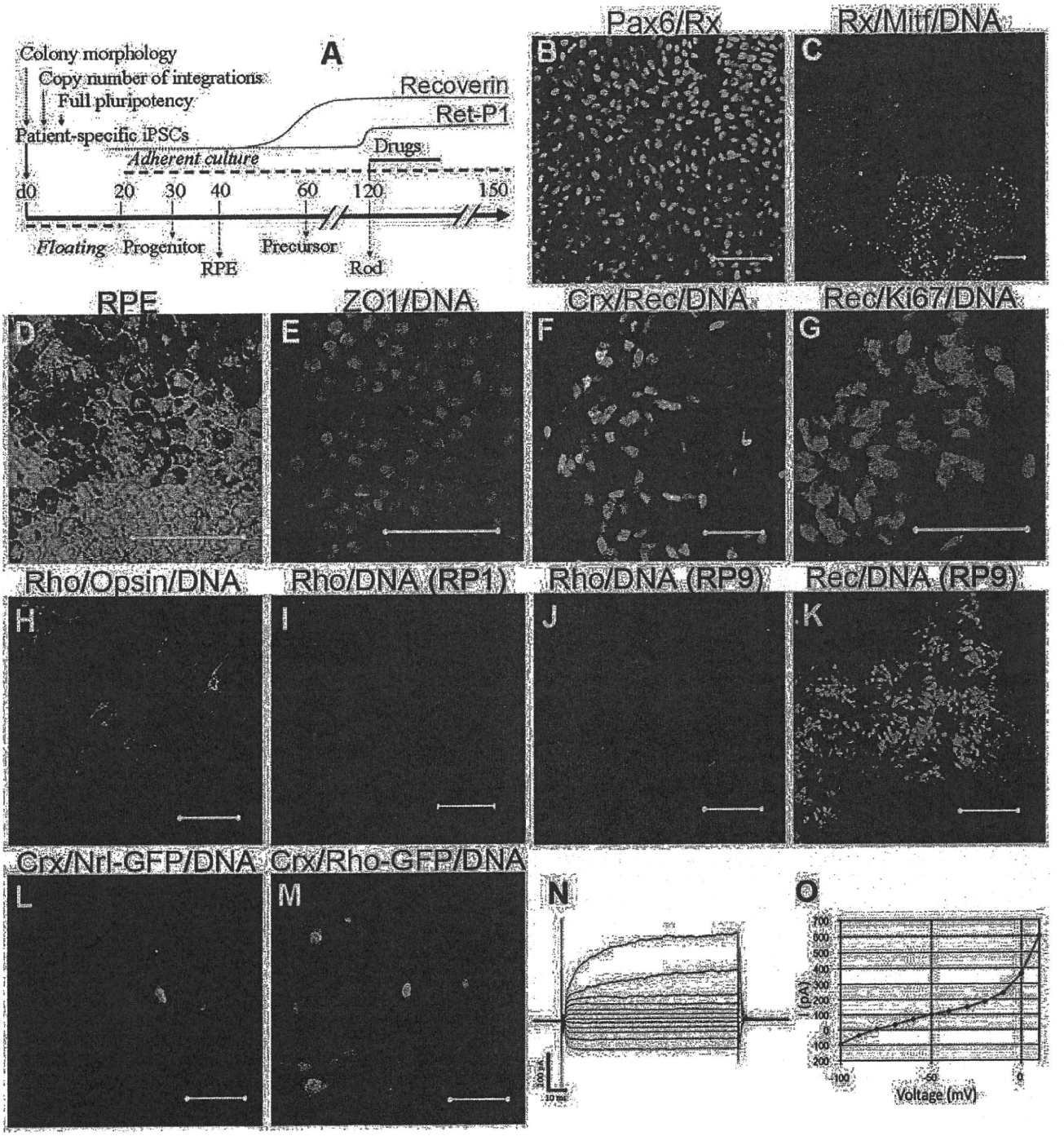

Figure 2. Induction of patient-specific retinal photoreceptor cells. Retinal cells were induced sequentially by *in vitro* differentiation. (**A**) Experimental schema. (**B**) Neural retina progenitor cells (Pax6+Rx+) and RPE progenitor cells (Mitf+) were separated in the culture dish (**C**). Patient-specific RPE cells exhibited hexagonal morphology and pigmentation (**D**) and expressed the tight junction marker ZO-1 (**E**). Photoreceptor cells were positive for immature photoreceptor markers Crx and Recoverin on day 60 (**F**). Recoverin+ cells did not co-express Ki67, a proliferating cell marker (**G**). Differentiation of rod photoreceptors (Rhodopsin+) and cone photoreceptors (Opsin+) from patient iPS cells (**H**). Rhodopsin + rod photoreceptors induced from K21-iPS at day 120 (**I**). K11-derived rod photoreceptors were observed at day 120 (**J**). No Rhodopsin+ cells were detected, but Recoverin+ cells were present at day 150(**K**). Induced rod photoreceptor cells (Crx+) labeled with lentiviral vectors encoding GFP driven by a rod photoreceptor-specific promoter Nrl (**L**: Nrl-GFP) or Rhodopsin (**M**: Rho-GFP). Arrows indicate cells co-expressing Crx and GFP. (**N**) Whole-cell recording of rod photoreceptor cell differentiated human iPS cells. Recorded cells expressed GFP under the control of the Rhodopsin promoter. (**O**) Relationship between voltage and membrane current (i) produced a non-linear curve, suggesting that voltage-dependent channels exist in iPS cell-derived rod photoreceptors Rec, Recoverin; Rho, Rhodopsin. Scale bars, 50 μm.
doi:10.1371/journal.pone.0017084.g002

(data from three selected lines), consistent with stable differentiation. Furthermore, we confirmed rod induction by labeling with lentiviral vectors driving GFP from the Rhodopsin and Nrl promoters, either of which is specifically expressed in rod photoreceptors (**Fig. 2L–M**). Whole-cell patch-clamp recording demonstrated that the rod photoreceptor cell membrane contains voltage-dependent channels, suggesting that differentiated patient-derived rod cells are electrophysiologically functional (**Fig. 2N–O**). Meanwhile, the excluded iPS cell lines (ones that showed spontaneous differentiation during maintenance, or had a high copy number of transgenes), demonstrated a significant diversity of differentiation (**Fig. S7**). Together, these data show that patient-derived iPS cells can differentiate into cells that exhibit many of the immunochemical and electrophysiological features of mature rod photoreceptor cells.

Patient-specific rod cells undergo degeneration *in vitro*

As compared with normal iPS cells, there is no significant difference in rod cell differentiation efficiency at day 120 in K21(RP1)-, P101(PRPH2)-, and P59(RHO)-iPS cell lines (**Fig. 3**). iPS cells from both K11(RP9) and K10(RP9) carried a RP9 mutation; however, rod cell number was significantly lower than in normal iPS cells (**Fig. 3**). We asked whether early death of precursor cells leads to a smaller number of mature rod photoreceptor cells. To determine whether genetic mutations induce degeneration in photoreceptors cells *in vitro*, we extended the culture period and evaluated the number of rod photoreceptors at day 150. In differentiated iPS cells from patient K21(RP1) at day 150, the number of Rhodposin+ cells was significantly decreased (**Fig. 3**). For the K11-iPS cells, no Rhodposin+ cells were found at day 150 (**Fig. 3**). Importantly, some K11-cells at day 150 were positive for Recoverin (10.3±1.99%) and Crx, markers for the rod, cone photoreceptors, and/or bipolar cells (**Fig. 2K** and data not shown), strongly suggesting that cone photoreceptor and/or bipolar cells survived, whereas the rod photoreceptors underwent degeneration *in vitro*. In addition, we detected cells positive for Islet1 (a marker for retinal amacrine, bipolar and ganglion cells), again consistent with the survival of other types of retinal cells (**Fig. S6F**). From these results, we concluded that mature rod photoreceptors differentiated from patient iPS cells selectively degenerate in an RP-specific manner *in vitro*.

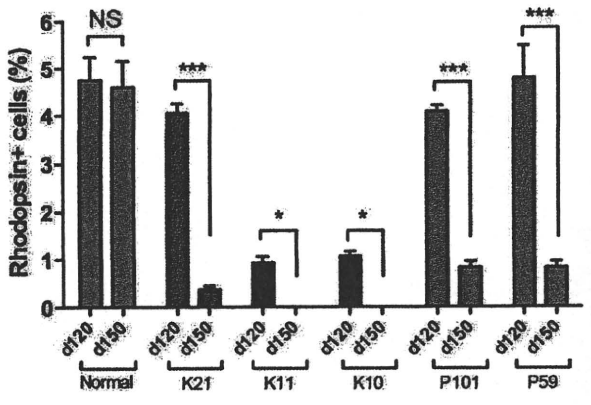

Figure 3. RP patient-derived rod photoreceptors undergo degeneration *in vitro*. iPS cells were differentiated into Rhodopsin+ rod photoreceptors in serum-free culture of embryoid body-like aggregates (SFEB culture). The percentages of Rhodopsin+ rod photoreceptors were evaluated at both day 120 and day 150, respectively. Data were from three independent iPS cell lines derived from the patients. ANOVA followed by Dunnett's test. * $p<0.05$; *** $p<0.001$. Values in the graphs are means and s.e.m.
doi:10.1371/journal.pone.0017084.g003

Cellular stresses involved in patient-derived rod cells

We next asked how the patient-derived rod photoreceptors degenerate. We evaluated apoptosis and cellular stresses in each cell line at both day 100 and day 120, respectively. Interestingly, in the RP9-iPS (K10 and K11) cells, a subset of Recoverin+ cells co-expressed cytoplasmic 8-hydroxy-2'-deoxyguanosine (8-OHdG), a major oxidative stress marker, indicating the presence of DNA oxidation in RP9 patient-derived photoreceptors by differentiation day 100 (**Fig. 4A** and **Fig. S8**). More caspase-3+ cells were presented in the Crx+ photoreceptor cluster of RP9-iPS than in those from other lines (**Fig. 4C–D**). After maturation of the rod photoreceptors from RP9-iPS cells, Rhodopsin+ cells co-expressed Acrolein, a marker of lipid oxidation (**Fig. 4E**), while no Rhodopsin+/Acrolein+ cells were observed in iPS cells derived from other patients carrying different mutations or in normal iPS cells (**Fig. 4F**). This pattern was similar to the cases of 8-OHdG and activated caspase-3. Thus, we conclude that oxidation is involved in the RP9-rod photoreceptor degeneration.

In differentiated RHO-iPS (P59) cells, we found that Rhodopsin proteins were localized in the cytoplasm (**Fig. 4G**), as determined by immunostaining with anti-Rhodopsin antibody (Ret-P1). This pattern is unlike the normal localization of Rhodopsin at the cell membrane in photoreceptors derived from normal iPS or other patient-derived iPS cells (**Fig. 4H** and data not shown). This result suggests accumulation of unfolded Rhodopsin, as reported previously in rhodopsin mutant mice cells [13]. We next examined the possible involvement of endoplasmic reticulum (ER) stress in RHO-iPS cell line degeneration. The Rhodopsin+ or Recoverin+ cells co-expressed immunoglobulin heavy-chain binding protein (BiP) or C/EBP homologous protein (CHOP), two conventional markers of endoplasmic reticulum (ER) stress, from day 120 (**Fig. 4I,K and Fig. S9**), while cells derived from control iPS or other mutant iPS cells were negative for BiP and CHOP (**Fig. 4J,L**). Taken together, these results demonstrate that ER stress is involved in rod photoreceptors carrying a RHO mutation.

Drug evaluation in patient-specific rod cells

The antioxidant vitamins α-tocopherol, ascorbic acid, and β-carotene have been tested in clinical trials as dietary therapies for RP [2] and in another major retinal degenerative disease, age-related macular degeneration [14]. Thus far, mostly due to the lack of appropriate validation models, there has been no evidence supporting the beneficial effects of these compounds on rod photoreceptors. We therefore assessed the effects of these agents on rod photoreceptors derived from patient iPS cells. In mouse retinal culture, short-term treatment with α-tocopherol, ascorbic acid and β-carotene at 100 μM, 200 μM and 1.6 μM, respectively, exerted no significant toxic effects on rod photoreceptor cells (**Fig. S10**). Since the differentiated rod photoreceptors underwent degeneration after day 120, we treated the cells for 7 days with these agents starting at day 120 (**Fig. 2A**). α-Tocopherol treatment significantly increased the number of Rhodopsin+ cells in iPS cells derived from K11- and K10-iPS with the RP9 mutation, while it had no significant effects on iPS cells with the either the RP1, PRPH2 or RHO mutation (**Fig. 5**). In contrast, neither ascorbic acid nor β-carotene treatment had any effect on iPS cells of any genotype (**Fig. S11**). We cannot currently explain the discrepancy between the effects of these antioxidants. It has been reported that under certain circumstances, anti-oxidants can act as "pro-oxidants" [15]. Taken together, our results indicate that treatment with α-tocopherol is beneficial to RP9-rod photoreceptor survival, and causes different effects on Rhodposin+ cells derived from different patients.